Environmental Science Nano

PAPER

View Article Online
View Journal | View Issue

CrossMark click for updates

Cite this: *Environ. Sci.: Nano*, 2016, 3, 94

Extremely high arsenic removal capacity for mesoporous aluminium magnesium oxide composites†

Wei Li,‡[a] Dehong Chen,[b] Fang Xia,[ac] Jeannie Z. Y. Tan,[ab] Pei-Pei Huang,[d] Wei-Guo Song,[d] Natalita M. Nursam[ab] and Rachel A. Caruso*[ab]

Received 7th August 2015,
Accepted 12th October 2015

DOI: 10.1039/c5en00171d

rsc.li/es-nano

Published on 21 October 2015. Downloaded on 18/03/2016 08:24:55.

Mesoporous aluminium magnesium oxide composites with varying composition (Mg content: 0–100%) and high surface area (118–425 m^2 g^{-1}) are synthesized by a facile, low-cost and scalable sol–gel method. The mesostructure and crystallinity are controlled by varying the composition and calcination temperature. The mesopores evolve from hexagonally ordered to wormhole-like in structure with increasing Mg/Al ratio. The mesoporous aluminium magnesium oxide composites are highly efficient adsorbents for removing As(v) and As(iii) from water. The mesoporous magnesium oxide shows unprecedentedly high adsorption capacities of 912 mg g^{-1} for As(v) at pH 3 and 813 mg g^{-1} for As(iii) at pH 7 with a dose of 0.5 g L^{-1}; significantly higher than those of reported adsorbents. Exceptional adsorption capacities for arsenic are retained over a wide pH range, and high selectivity for As(v) is realized even in the presence of co-existing anions. The arsenic adsorption performance correlates to the properties of the composites including the Mg/Al ratio, point of zero charge, crystallinity and mesostructure. The arsenic adsorption mechanism is elucidated. Due to their high surface areas, large pore volumes, tunable mesopore structures and high quantities of accessible hydroxyl groups with strong chemisorption binding affinity to arsenic, as well as extremely high adsorption capacities and selectivity, these mesoporous aluminium magnesium oxides are promising adsorbent candidates for the remediation of arsenic in water.

Nano impact

Arsenic pollution in water causes serious environmental and health concerns. Adsorption is an effective approach to remove arsenic from water. The challenge lies in developing efficient adsorbents with high adsorption capacities and excellent selectivity for As(v) and As(iii). Understanding how the material properties correlate with adsorption performance is essential for the rational design of efficient adsorbents. Here we present a sol–gel approach to produce mesoporous aluminium magnesium oxide composites. With increasing Mg/Al ratios, the composite structures evolved from ordered nanopores to nanoparticle-composed networks, with high surface areas. Extremely high adsorption capacities for arsenate and arsenite, along with excellent selectivity, were exhibited.

Introduction

Heavy metal ions, existing in natural underground water or released into drinking water resources by industry are causing environmental and public health concerns.[1–8] Arsenic contamination in natural water poses a severe threat to global health due to its high toxicity and carcinogenicity. The arsenic provisional guideline level in drinking water is 10 ppb, according to the World Health Organization (WHO).[9] However, arsenic concentrations in groundwater in areas of Australia, China, USA, Bangladesh, India and South America exceed 10 ppb.[10–12] About 140 million people in the world are drinking groundwater containing arsenic above this level.[13] Chronic exposure to the arsenic-contaminated water can lead

[a] *CSIRO Manufacturing, Clayton South, Victoria, 3169, Australia*
[b] *Particulate Fluids Processing Centre, School of Chemistry, The University of Melbourne, Melbourne, Victoria, 3010, Australia.*
E-mail: rcaruso@unimelb.edu.au
[c] *School of Engineering and Information Technology, Murdoch University, Murdoch, West Australia, 6150, Australia*
[d] *Beijing National Laboratory for Molecular Sciences (BNLMS), Institute of Chemistry, Chinese Academy of Sciences, Beijing, 100190, PR China*

† Electronic supplementary information (ESI) available: Physical properties, arsenic adsorption kinetic and isotherm parameters of mesoporous aluminium magnesium oxides, effect of co-existing anions on As(v) adsorption, TEM images, XRD patterns, XPS and FTIR spectra of adsorbents before and after adsorption. See DOI: 10.1039/c5en00171d

‡ Present address: International Iberian Nanotechnology Laboratory (INL), Avenida Mestre José Veiga, Braga, 4715-330, Portugal.

This journal is © The Royal Society of Chemistry 2016

Published on 21 October 2015. Downloaded on 18/03/2016 08:24:55.

to adverse health effects such as arsenicosis, skin lesions, and lung, bladder, and kidney cancers.[14–16]

Arsenic mainly exists as arsenate (As(v)) and arsenite (As(III)) in natural water.[17] As(v) is the dominant species in alkaline and oxidizing groundwater in the form of oxyanions ($H_2AsO_4^-$ and $HAsO_4^{2-}$), while As(III) is predominant in the moderately reducing aqueous environment as neutral H_3AsO_3.[13,18,19] Compared to As(v), As(III) is much more toxic and difficult to remove from water due to its weaker affinity to the surface of adsorbents, which results in low As(III) adsorption capacity on most adsorbents.[20,21] The removal capacity of As(III) and As(v) is influenced by the redox conditions, pH and the presence of complex ions in water. As a result, pre-treatment processes prior to water purification, such as oxidation of As(III) to As(v) and pH adjustment are often required to achieve effective removal of arsenic.[20,22] However, these pre-treatment processes are costly and time-consuming, and may lead to secondary pollution. Therefore, developing efficient technologies to remove arsenic from water is of vital significance and has attracted considerable research efforts.

During the past decades, various water purification methods have been developed to remove arsenic. These methods include chemical precipitation, coagulation, ion-exchange, adsorption, ultrafiltration, electrochemical treatments and reverse osmosis.[5,23–25] Among these technologies, the adsorption technique is considered to be one of the most straightforward and promising approaches, due to its ease of operation, simple unit assembly, low cost and high efficiency.[4] A wide range of hierarchically nanostructured adsorbents have been reported for the adsorption of arsenic, such as carbon nanospheres,[26] Fe_2O_3,[27] FeOOH,[28,29] TiO_2,[30] Fe_3O_4,[31,32] CeO_2,[33] and CuO,[34] as well as composite adsorbents of Fe_3O_4/graphene,[35] Fe_2O_3/silica,[20] briquette/Fe_3O_4/MnO_2,[36] ZrO_2/carbon nanotubes,[37] titanium lanthanum oxide/activated carbon,[38] and AlOOH/Fe_3O_4.[39] However, many of these adsorbents exhibit relatively low adsorption capacities, and suffer from low synthesis yield and high cost.[27,40] Some are likely to cause secondary pollution or fail to remove arsenic in the presence of complex co-existing ions or at low pH values.[34,36] These issues dramatically restrict the large-scale production and application of nanostructured adsorbents. Therefore, it is highly desirable to develop effective adsorbents that exhibit excellent adsorption capacities for arsenic with selectivity using a facile, scalable and low-cost approach.

Porous materials are promising adsorbent candidates as accessibility to the large surface area of the porous structure can offer fast mass transfer. This, along with a large number of active adsorption sites, gives rise to high adsorption capacities for arsenic.[8,20] Porous alumina and magnesia have been widely used in water treatment, due to their low cost, natural abundance and relatively good adsorption performance.[41,42] For example, the commercial activated alumina (AA) is perhaps the most frequently adopted adsorbent. However, the As(v) adsorption capacity of AA is only 12 mg g^{-1}.[43] Kim *et al.* prepared mesoporous alumina that exhibited enhanced arsenic adsorption capacity.[18] Li *et al.* reported highly ordered mesoporous Ca-doped alumina that showed super adsorption capacities for arsenic and fluoride.[8] As a nontoxic and environmentally benign adsorbent, MgO is also widely used in practical water treatment.[22,44,45] Since the pH of the zero point of charge (pH_{zpc}) is 12.4, MgO is usually utilized as an anion adsorbent because of favorable electrostatic attraction.[22,46] However, the yield and adsorption capacity of reported nanostructured MgO adsorbents could be improved to meet the demand of mass production in practical application.[22,44] To fully exploit the functionality of alumina and magnesia in water treatment, studies examining the correlation of the material properties with their adsorption performance are essential. Furthermore, unravelling the adsorption mechanism is important for the rational design and synthesis of highly efficient adsorbents for arsenic removal.

In this study, mesoporous alumina, magnesia and their composites were synthesized by a facile, reproducible and high-yield method and studied as highly efficient adsorbents for removing As(v) and As(III) from water. The aluminium magnesium oxide compositions were varied from 0 to 100% Mg, giving high surface areas (118–425 m^2 g^{-1}). Transmission electron microscope (TEM) images and synchrotron small angle X-ray scattering (SAXS) patterns demonstrated the evolution of the mesopores from uniform hexagonally ordered to wormhole-like structures with increasing Mg/Al ratio. The arsenic adsorption performance could be correlated to the properties of the aluminium magnesium oxide composites, such as the Mg/Al ratio, pH_{zpc}, crystallinity and mesostructure. The mesoporous aluminium magnesium oxide composites showed extremely high adsorption capacities for As(v) and As(III). Exceptional adsorption capacities for arsenic were retained over a wide pH range, and high selectivity for As(v) was observed even in the presence of co-existing anions. A possible arsenic adsorption mechanism was hypothesised.

Experimental section

Materials

Pluronic P123 (M_n = 5800, $EO_{20}PO_{70}EO_{20}$), aluminium isopropoxide (>98 wt%), Na_2SiO_3, and Na_3PO_4 were purchased from Sigma-Aldrich. $Mg(NO_3)_2{\cdot}6H_2O$, $Na_2HAsO_4{\cdot}7H_2O$, $NaAsO_2$, HNO_3 solution (69 wt%), and NaCl were obtained from Merck. $NaNO_3$, Na_2SO_4, and Na_2CO_3 were purchased from BDH Chemicals VWR. All chemicals and solvents were used as received. Milli-Q water (18.2 MΩ cm) was used for solution preparation and synthesis.

Synthesis of adsorbents

The mesoporous alumina, magnesium oxides and the composites were synthesized by a sol–gel route with block copolymers as soft templates, by adapting a process developed by Yuan *et al.* for mesoporous alumina.[41] In a typical synthesis procedure, 10.0 g of Pluronic P123 was dissolved in 200.0 mL of anhydrous ethanol at room temperature and stirred for 1

Published on 21 October 2015. Downloaded on 18/03/2016 08:24:55.

h. Then 16 mL of 69 wt% nitric acid and 100 mmol of aluminium isopropoxide or $Mg(NO_3)_2{\cdot}6H_2O$ were added with vigorous stirring. After stirring for 5 h, the solution was put in an oven at 60 °C to undergo solvent evaporation. After 2 days, light yellow solid samples were obtained. The resulting powder samples were heated to 400 °C in a furnace at a slow ramp rate of 1 °C min^{-1} and kept at 400 °C for 4 h in air. To obtain the crystalline products, further high-temperature calcination at 900 °C was carried out in air for 1 h using a rapid ramp rate of 10 °C min^{-1}. After naturally cooling to room temperature, the mesoporous composites were collected and kept in an oven at 60 °C. For the syntheses of mesoporous aluminium magnesium oxide composites, aluminium isopropoxide and $Mg(NO_3)_2{\cdot}6H_2O$ were added to the Pluronic/ethanol/nitric acid solution with vigorous stirring at varying Al/Mg molar ratios. The total quantity of metal species was fixed at 100 mmol and the Al/Mg molar ratio was varied from 3/7 to 9/1. Other synthetic conditions remained identical. The calcined composite samples were denoted as meso-*x*Al(100 − *x*)Mg-*T*, where x = Al × 100/(Al + Mg) in molar ratio based on synthesis quantities and T was the final calcination temperature and meso represented mesoporous. The as-synthesized adsorbent powders were stored in air at 60 °C.

Batch adsorption tests

All the adsorption experiments were carried out at room temperature using polypropylene (PP) vessels. The stock solutions (*ca.* 1000 mg L^{-1}) of As(v) and As(iii) were prepared and then diluted to various concentrations. The initial pH of the arsenic solutions were adjusted as required with 1 M HCl or NaOH. The adsorption isotherms of As(v) and As(iii) on the mesoporous composite adsorbents were obtained using a batch contact methodology in which the adsorbent powder was magnetically stirred in solutions of a dose of 0.5 g L^{-1} (a commonly used dose in previous works).[26,28,29,32,51] In a typical procedure to obtain the adsorption isotherm of As(v), 0.02 g adsorbent was suspended in 40 mL of As(v) solution in a screw-capped PP vessel with various initial concentrations ranging from 10 to 1000 mg L^{-1}. The initial pH of the As(v) solution was adjusted to 3.0 ± 0.1. After stirring (300 rpm) for 48 h, the adsorbents were removed by using a syringe filter with a 0.22 μm hydrophilic polyethersulfone membrane (Millipore Millex) and further by centrifugation at 12 000 rpm. The arsenic concentrations of the filtrates and initial solutions were measured. The adsorption capacity, Q_e (mg g^{-1}), of the adsorbent was calculated based on the following equation:

$$Q_e = (C_0 - C_e) \times V/m$$

where C_0 (mg L^{-1}) and C_e (mg L^{-1}) represent the initial and equilibrium arsenic concentrations, respectively. V (L) is the volume of the arsenic solution and m (g) is the mass of adsorbent. The As(iii) adsorption isotherm tests were performed in a similar way, except that the initial pH was 7.0 ± 0.1.

To investigate the effect of initial pH on the adsorption capacity of As(v) and As(iii) over the adsorbents, the initial pH was varied from 2 to 12 and the initial arsenic concentration was fixed at 400 mg L^{-1}, while other conditions remained the same. To study the effect of co-existing anions on the As(v) uptake of adsorbents, six As(v) solutions (50 mg L^{-1}) were prepared with an initial pH of 6.0, containing either 10 mg L^{-1} of NO_3^-, 200 mg L^{-1} of Cl^-, 200 mg L^{-1} of SO_4^{2-}, 50 mg L^{-1} of CO_3^{2-}, 50 mg L^{-1} of SiO_3^{2-} or 50 mg L^{-1} of PO_4^{3-} by using their respective sodium salts. The concentrations of these co-existing competing anions were used based on their maximum contaminant levels from the U.S.A. Environmental Protection Agency and WHO.[1,9]

For the kinetic study of As(v) adsorption on various adsorbents, 0.25 g of adsorbent was dispersed in 500 mL of a 103 mg L^{-1} As(v) solution with an initial pH of 3.0. At predetermined time intervals, 5 mL of solution was collected and quickly filtered, and then the arsenic concentration was measured. All the adsorption experiments were repeated three times and the mean values were reported. The relative errors of the data were about 10%.

Characterization

The products were characterized by high resolution transmission electron microscopy (HRTEM, FEI Tecnai F20), powder X-ray diffraction (XRD, Bruker D8 diffractometer with Cu Kα radiation at 40 kV and 40 mA), X-ray photoelectron spectroscopy (XPS, ESCALab220i-XL electron spectrometer from VG Scientific using 300W Al Kα radiation), and Fourier-transform infrared spectroscopy (FTIR, Nicolet 6700 FT-IR spectrometer). Small angle X-ray scattering (SAXS) patterns of the samples were recorded at 12 keV on the SAXS beamline at the Australian Synchrotron. The pH values of zero point of charge (pH_{zpc}) of the adsorbents were measured using the Malvern Nano series zeta potential instrument. Nitrogen gas sorption isotherms were measured at −196 °C on a Micromeritics Tristar 3000 surface area and porosity analyzer. All samples were degassed at 160 °C on a vacuum line for 12 h prior to the measurements. The specific surface area and pore size were calculated using the Brunauer–Emmett–Teller (BET) and Barrett–Joyner–Halenda (BJH) method, respectively. The arsenic concentration was measured by inductively coupled plasma optical emission spectroscopy (ICP-OES, Varian 730-ES Simultaneous Axial ICP-OES).

Results and discussion

Materials synthesis and characterization

A series of mesoporous aluminium magnesium oxide composites with tunable molar ratios of Mg/Al were fabricated by a simple and scalable sol–gel method with the block copolymer P123 as the soft template. The compositions could be varied from 0 to 100% Mg. The precursor materials obtained from the sol–gel process were calcined at 400 °C or 900 °C to produce two sets of mesoporous aluminium magnesium oxide composites with amorphous and crystalline phases,

 This journal is © The Royal Society of Chemistry 2016

Published on 21 October 2015. Downloaded on 18/03/2016 08:24:55.

respectively. In a typical experiment, over 10 g of mesoporous aluminium magnesium oxide was produced in one batch (Fig. S1, ESI†). The morphology and porous structures of these composites were studied by TEM. Fig. 1 displays the evolution of the mesopore structures from uniform hexagonally ordered to wormhole-like with increasing Mg/Al ratio. For the composite samples containing up to 30% Mg (from meso-Al-400 to meso-70Al30Mg-400), the uniform hexagonally ordered mesopores have a *p6mm* symmetry. The alignment of cylindrical mesopores along the [110] direction is clear in Fig. 1a–d.[41,42] The sizes of these hexagonally ordered mesopores are in the range of 10–15 nm. However, the mesopores in samples with higher Mg contents (from meso-50Al50Mg-400 to meso-Mg-400) are disordered and have a wormhole-like structure with the network being composed of nanoparticles (Fig. 1e–g). These small irregular nanoparticles have an average diameter of 6–10 nm and assembled to a nanoporous network with little agglomeration, despite the small size (Fig. S2 a–f, ESI†). After calcination at 900 °C, the ordered mesoporous framework was retained in the samples of meso-Al-900 (Fig. 1h) as well as meso-90Al10Mg-900 and meso-80Al-20Mg-900 (Fig. S2 g–i, ESI†). Most of the original hexagonally ordered mesopores in meso-70Al30Mg-400 collapsed due to the formation of nanoparticles with an average size of *ca.* 20 nm after calcination at 900 °C, yet without severe aggregation (Fig. S2 j and k, ESI†). For comparison, the alumina sample (Al-400) was also prepared without using the P123 template. The amorphous Al-400 sample did not contain any mesopores (Fig. S3, ESI†) and was used as the control sample in the adsorption experiments.

Synchrotron SAXS patterns were collected to track the mesostructured evolution in the mesoporous aluminium magnesium oxides with increasing Mg/Al ratio.

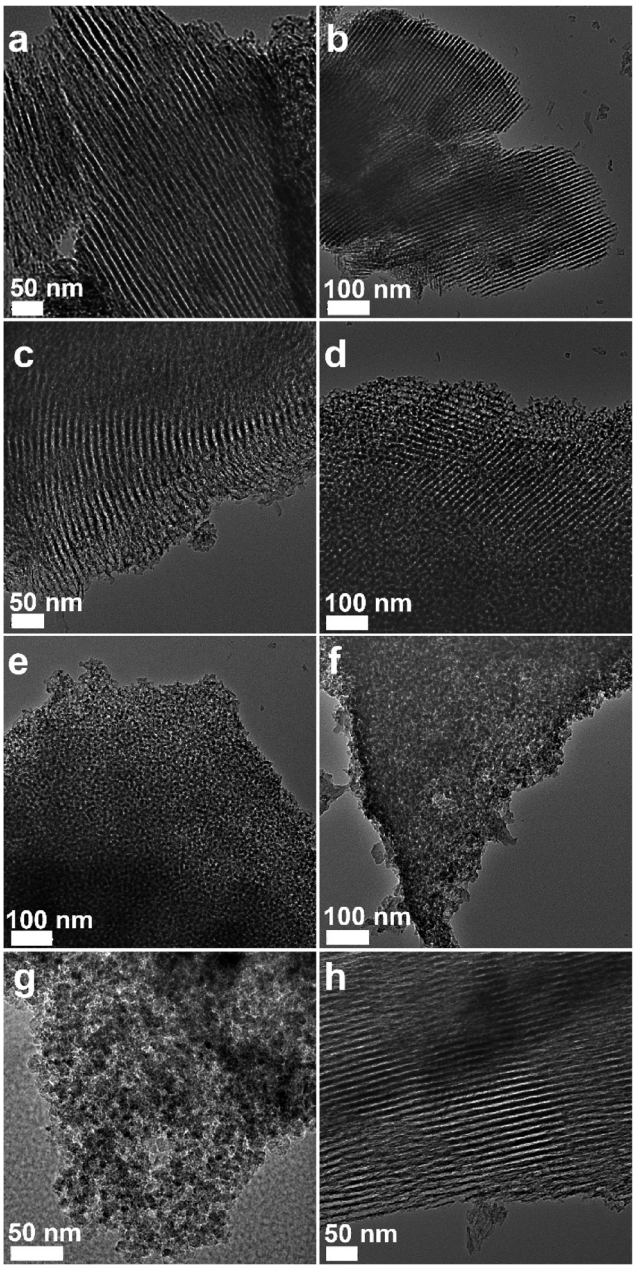

Fig. 1 TEM images of (a) meso-Al-400, (b) meso-90Al10Mg-400, (c) meso-80Al20Mg-400, (d) meso-70Al30Mg-400, (e) meso-50Al50Mg-400, (f) meso-30Al70Mg-400, (g) meso-Mg-400 and (h) meso-Al-900.

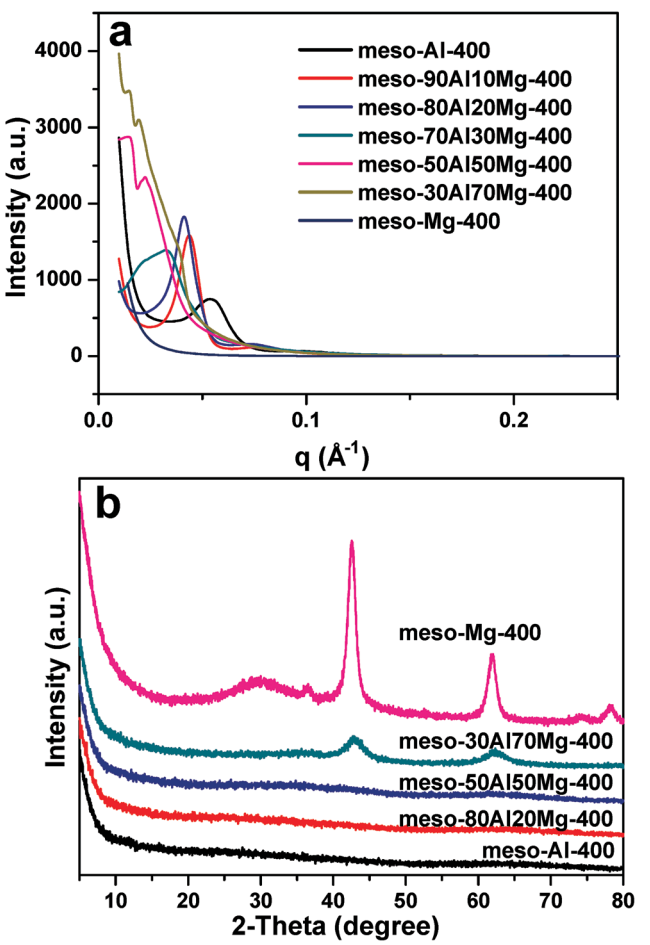

Fig. 2 (a) Synchrotron SAXS and (b) wide angle XRD patterns of mesoporous aluminium magnesium oxide samples with varying Mg/Al molar ratios and calcined at 400 °C.

Published on 21 October 2015. Downloaded on 18/03/2016 08:24:55.

Fig. 2a shows the synchrotron SAXS patterns of all samples calcined at 400 °C. A well-defined peak can be seen in the SAXS patterns of the samples from meso-Al-400 to meso70Al30Mg-400, indicating the presence of hexagonally ordered mesopores. With further increasing content of Mg in the composite samples, the peak becomes weaker and vanishes for the pure mesoporous magnesia (meso-Mg-400). The synchrotron SAXS results confirm the evolution of mesostructures from hexagonally ordered to wormhole-like with increasing Mg/Al ratio, in excellent agreement with TEM observation.

Composites containing less than 70% Mg (from meso-Al-400 to meso-50Al50Mg-400) and calcined at 400 °C are amorphous, as shown in the powder X-ray diffraction (XRD) patterns (Fig. 2b). The diffraction peaks in the XRD patterns of both meso-30Al70Mg-400 and meso-Mg-400 were indexed to the cubic phase of MgO (JCPDS Card No. 45-0946). Calcination at 900 °C caused crystallization. Fig. S4 (ESI†) shows the synchrotron SAXS and XRD patterns of the samples calcined at 900 °C. The SAXS patterns of meso-Al-900 and some composites confirm the retention of robust hexagonally ordered mesoporous frameworks after calcination at 900 °C, consistent with the TEM observation (Fig. S2, ESI†). The meso-Al-400 was converted to the γ-Al_2O_3 phase (JCPDS Card No. 10-0425) after calcination at 900 °C. For samples of meso-*x*Al(100 − *x*)Mg-900 (*x* = 30–90), the XRD patterns (Fig. S4b, ESI†) can be assigned to distinct $MgAl_2O_4$ spinel phases along with γ-Al_2O_3.[42] Besides the presence of $MgAl_2O_4$ phases, the cubic MgO phase also exists in meso-50Al50Mg-900 and meso-30Al70Mg-900, as summarized in Table S1, ESI.†

The elemental composition of the composites (meso-Al-400, meso-80Al20Mg-400 and meso-Mg-400) was confirmed by XPS (Fig. S5, ESI†). The XPS of meso-80Al20Mg-400 reveals the presence of Al, O, Mg and C. The elemental quantitative analysis demonstrates that the atomic ratio of Mg/Al is 0.22, consistent with the inductively coupled plasma optical emission spectroscopy (ICP-OES) result of 0.24.

Nitrogen gas sorption analyses were carried out to study the porosity of the composites. Fig. 3 illustrates the nitrogen sorption isotherms and corresponding pore size distribution curves of the composites calcined at 400 °C. Most of the isotherms are type IV curves, characteristic of mesoporous materials (Fig. 3a).[41,42,47] Table 1 summarizes the Brunauer–Emmett–Teller (BET) surface areas, pore sizes and pore volumes calculated by the Barrett–Joyner–Halenda (BJH) method, as well as their pH_{zpc} and crystallinity of the composite samples calcined at 400 °C. All the samples exhibit high surface areas, uniform mesopores and large pore volumes. These features are favorable for adsorption, as they provide high quantities of active adsorption sites and facilitate fast mass transfer for the arsenate or arsenite adsorption.[18,22,36,38] The pore size of these adsorbents is larger than the diameter of the arsenic species ($HAsO_4^{2-}$: 7.94 Å, $H_2AsO_4^-$: 8.32 Å, H_3AsO_4: 8.32 Å, $H_2AsO_3^-$: 9.60 Å and H_3AsO_3: 9.60 Å).[18] Therefore, while the arsenic species could adsorb onto the outer surface of the samples it can also diffuse into the pore channels and bind to the inner surface of the mesopores.[48] Owing to their hexagonally ordered mesopores, the aluminium magnesium oxides with <50% Mg (from meso-Al-400 to meso70Al30Mg-400) exhibit higher surface areas (>350 $m^2\ g^{-1}$) and larger pore volumes (>0.9 $cm^3\ g^{-1}$). The highest BET surface area of 424.9 $m^2\ g^{-1}$ was achieved for meso-90Al10Mg-400. The pore size distribution curves (Fig. 3b) demonstrate that the pore size rises gradually with increasing Mg contents from the pure meso-Al-400 sample to meso-50Al50Mg-400. However, the pore size drops dramatically to ~4.2 nm for the samples meso-30Al70Mg-400 and meso-Mg-400, probably due to the formation of the nanocrystalline MgO phase in these samples as identified in the corresponding XRD patterns (Fig. 2b). The nitrogen sorption results are in good agreement with TEM and SAXS characterization. In contrast to meso-Al-400, the sample of Al-400 prepared without using the P123 template exhibits a low BET surface area of only 53.8 $m^2\ g^{-1}$ (Fig. S3c, ESI†). Fig. S6 (ESI†)

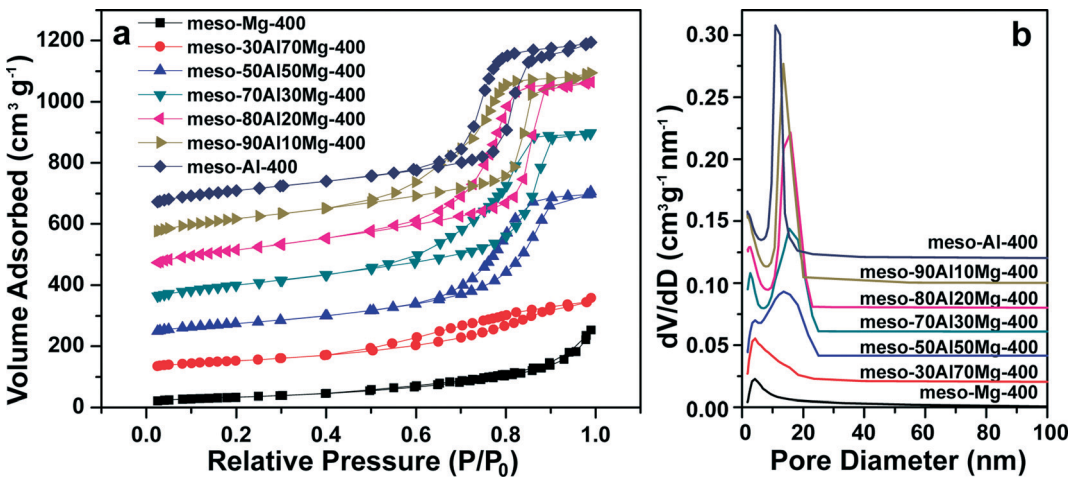

Fig. 3 (a) Nitrogen gas sorption isotherms of the mesoporous aluminium magnesium oxides with varying Mg/Al molar ratios and calcined at 400 °C and (b) the corresponding pore size distribution derived from the adsorption branches on the basis of the BJH model. Each subsequent curve is shifted up the *y* axis by 100 $cm^3\ g^{-1}$ in (a) and 0.02 $cm^3\ g^{-1}\ nm^{-1}$ in (b), for clarity.

 This journal is © The Royal Society of Chemistry 2016

Published on 21 October 2015. Downloaded on 18/03/2016 08:24:55.

Table 1 Physical properties of the mesoporous aluminium magnesium oxide composites calcined at 400 °C

Sample	S_{BET} [m^2 g^{-1}][a]	PSD [nm][b]	V_{sp} [cm^3 g^{-1}][c]	pH_{zpc}	Phase
Meso-Al-400	396.1	10.88	0.91	8.30	Amorphous
Meso-90Al10Mg-400	424.9	13.49	0.91	10.89	Amorphous
Meso-80Al20Mg-400	422.1	15.92	1.02	11.67	Amorphous
Meso-70Al30Mg-400	364.2	15.40	0.92	12.30	Amorphous
Meso-50Al50Mg-400	268.7	13.59	0.79	>12.98	Amorphous
Meso-30Al70Mg-400	187.3	4.27	0.38	>12.98	Cubic MgO
Meso-Mg-400	118.6	4.16	0.34	>13.00	Cubic MgO
Al-400	53.8	6.05	0.08	7.86	Amorphous

[a] S_{BET} = BET specific surface area obtained from nitrogen adsorption data in the P/P_0 range from 0.05 to 0.20. [b] PSD = pore size distribution determined by using the BJH method from the adsorption branch. [c] V_{sp} = single point pore volume calculated from the adsorption isotherm at P/P_0 = 0.98.

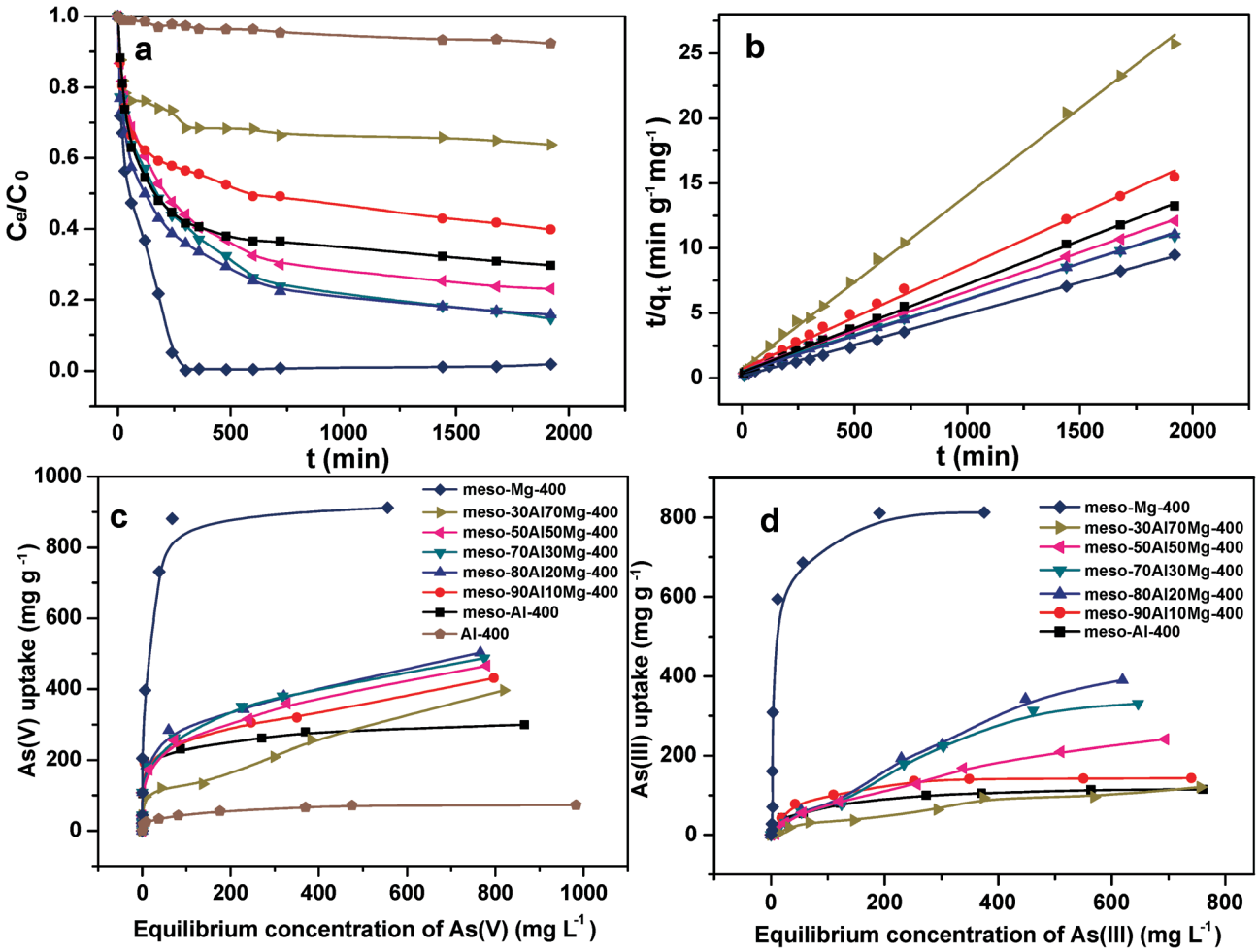

Fig. 4 (a) and (b) As(v) adsorption kinetics on aluminium magnesium oxides (the linear kinetic plots of meso-80Al20Mg-400 and meso-70Al30Mg-400 almost overlap in (b)); (c) and (d) adsorption isotherms of As(v) and As(iii) on the mesoporous aluminium magnesium oxides calcined at 400 °C, respectively. Legend for (a) is the same as shown in (c); and legend for (b) is the same as that of (d). Experimental conditions: dose = 0.5 g L^{-1}; for (a) and (b), initial pH = 3.0, C_0 (As(v)) = 103 mg L^{-1}; for (c) initial pH = 3.0, C_0 (As(v)) ranged from 10 to 1000 mg L^{-1}; for (d), initial pH = 7.0, C_0 (As(iii)) ranged from 10 to 1000 mg L^{-1}.

displays the nitrogen sorption isotherms and pore size distribution curves of all the samples calcined at 900 °C. The porous properties of the aluminium magnesium oxides calcined at 900 °C are summarized in Table S1 (ESI†); high temperature calcination reduces the surface areas.

Arsenic adsorption

Due to their high surface areas, abundance of mesopores (hexagonally ordered or wormhole-like) and high pore volumes, the aluminium magnesium oxide composites are

Published on 21 October 2015. Downloaded on 18/03/2016 08:24:55.

expected to show great potential in the adsorption of heavy metal ions for water purification. Arsenic was chosen to demonstrate the adsorption capability of the synthesized adsorbents. A series of studies were conducted to systematically explore the arsenic adsorption properties of the composites. Fig. 4a shows the As(v) adsorption kinetics of samples calcined at 400 °C. The adsorption process was very fast during the first 60 min and then slowed down gradually. The equilibrium was reached after 12 h for the samples of meso-Al-400 and the composites. The highest adsorption rate was achieved on meso-Mg-400. After 5 h, the As(v) concentration decreased from 103 to 0.1 mg L^{-1}, leading to an impressive adsorption capacity of 205 mg g^{-1} for the meso-Mg-400. The adsorption kinetic data fits the pseudo-second-order model well (Fig. 4b), indicating that the adsorption process occurred through chemical interactions.[20,22] The pseudo-second-order kinetic model is commonly expressed as

$$\frac{t}{q_t} = \frac{1}{q_e}t + \frac{1}{kq_e^2}$$

where q_e (mg g^{-1}) is the adsorption capacity at equilibrium, q_t (mg g^{-1}) is the amount of As(v) adsorbed at contact time t (min), and k (g mg^{-1} min^{-1}) is the rate constant of the pseudo-second-order model of adsorption. The fitting results are listed in Table S2, ESI.† The correlation coefficients, R^2, exceed 0.99 for all the mesoporous samples, suggesting that the pseudo-second-order model represents the As(v) adsorption kinetics over these mesoporous composite adsorbents. The rate constants are comparable to those of reported MgO nanoflakes and porous alumina under similar conditions.[18,44] The equilibrium adsorption capacity increases in the following order: Al-400 < meso-30Al70Mg-400 < meso-90Al10Mg-400 < meso-Al-400 < meso-50Al50Mg-400 < meso-80Al20Mg-400 < meso-70Al30Mg-400 < meso-Mg-400. The Al-400 sample exhibits the lowest adsorption capacity of 15.8 mg g^{-1}. Since Al-400 has the same amorphous phase as meso-Al-400 and was synthesized in a similar fashion except that P123 was not added, the lower As(v) uptake (15.8 mg g^{-1}) of Al-400 is due to its lower BET surface area and pore volume, highlighting the importance of porosity for mesoporous aluminium magnesium oxide composite adsorbents. In terms of the balance between adsorption rate constant and adsorption capacity, meso-Mg-400 shows the best adsorption performance in removing As(v) from water.

The maximum adsorption capacity is the most important indicator for the adsorbents. In order to evaluate the maximum adsorption capacities of the aluminium magnesium oxide adsorbents, the adsorption isotherms were obtained for initial arsenic concentrations of 10–1000 mg L^{-1}. Fig. 4c exhibits the typical adsorption isotherms of As(v) on all the samples calcined at 400 °C at an initial pH of 3.0. Several models have been established to analyse the adsorption isotherms. Among them, the Langmuir and Freundlich models are most commonly used for adsorption analysis.[49,50] The Langmuir model can be described as follows:

$$q_e = \frac{q_m b C_e}{1 + bC_e}$$

where C_e (mg L^{-1}) is the equilibrium concentration of ions; q_e (mg g^{-1}) is the mass of ions adsorbed per unit weight of the adsorbent at equilibrium; q_m (mg g^{-1}) is the maximum adsorption capacity corresponding to complete monolayer coverage and b is the equilibrium constant related to the adsorption energy. While the Freundlich model is described as:

$$q_e = K_F C_e^{1/n}$$

where the new terms K_F and n are the Freundlich constant related to the adsorption capacity and adsorption intensity, respectively. The parameters obtained for both the Langmuir and Freundlich models are listed in Table S3, ESI.† As displayed in Fig. 4c and Table S3 (ESI†) for meso-Al-400 and meso-Mg-400, the As(v) adsorption data fit the Langmuir model better. However, the Freundlich model is a better fit for the As(v) adsorption data of the composite samples.

The As(v) adsorption isotherms in Fig. 4c show that the highest As(v) adsorption capacity achieved for pure meso-Al-400 is 299 mg g^{-1} at the initial arsenic concentration of 1020 mg L^{-1}. This is much higher than previously reported values for metal oxide adsorbents, such as activated alumina,[43] mesoporous alumina,[18] ceria hollow nanospheres,[33] flower-like α-Fe_2O_3,[27] and urchin-like α-FeOOH hollow spheres.[28] The high adsorption capacity of meso-Al-400 is probably due to its highly ordered mesopores, high surface area and pore volume. By contrast, the control sample of Al-400 shows an adsorption capacity of merely 72 mg g^{-1}, because of its low BET surface area and pore volume. With increasing Mg content in the composite adsorbents, the adsorption capacity rises at first and then slightly decreases. The highest As(v) adsorption capacity of 503 mg g^{-1} is reached on the meso-80Al20-400 sample, which has a high BET surface area (422.1 m^2 g^{-1}) and the largest pore volume, as well as highly ordered cylindrical mesopores. Remarkably, pure meso-Mg-400 exhibits an exceptional adsorption capacity of 912 mg g^{-1} for As(v). To the best of our knowledge, this is the highest reported adsorption capacity for As(v) (Table 2). Many factors may contribute to this superior performance, including its high pH_{zpc} value (>13), strong bonding with arsenic species, and high surface area. This will be discussed later.

The mechanical strength or the macroscopic size of the resulting powders is important if the powders are to be loaded into a filter cartridge in practical water purification. The macroscopic size of the adsorbent powders became smaller with increasing Mg content, decreasing the mechanical strength. The pure meso-Mg-400 sample was composed of nanoparticles (6.69 nm) that required high-speed centrifugation to separate from water, while the meso-Al-400 sample with a bigger macroscopic size was easily filtered from water (Fig. S1, ESI†).

 This journal is © The Royal Society of Chemistry 2016

Published on 21 October 2015. Downloaded on 18/03/2016 08:24:55.

Table 2 Comparison of arsenic adsorption capacities on various adsorbents

Adsorbent	Concentration range [mg L^{-1}]	Dose [g L^{-1}]	Initial pH	As(v) uptake [mg g^{-1}]	As(iii) uptake [mg g^{-1}]	Reference
Meso-Al-400	0.1–1000	0.5	3.0	299	110 (at 400 mg L^{-1})	This work
Meso-Al-400	0.1–1000	0.5	7.0	120 (at 400 mg L^{-1})	115	This work
Meso-80Al20Mg-400	0.1–1000	0.5	3.0	503	217 (at 400 mg L^{-1})	This work
Meso-80Al20Mg-400	0.1–1000	0.5	7.0	225 (at 400 mg L^{-1})	391	This work
Meso-Mg-400	0.1–1000	0.5	3.0	912	615 (at 400 mg L^{-1})	This work
Meso-Mg-400	0.1–1000	0.5	7.0	485 (at 400 mg L^{-1})	813	This work
Flower-like Fe_2O_3	1–20	2	3	7.6	N/A	27
Urchin-like α-FeOOH hollow spheres	10–1000	0.5	7	58	N/A	28
Chrysanthemum-like α-FeOOH microspheres	10–1500	0.5	7	66.2	N/A	29
Activated alumina	0.02–12	1	2.6 (for As(v)) 7.0 (for As(iii))	12.34	3.48	43
γ-Fe_2O_3/macroporous silica	0.1–600	1	7	248	320	20
Mesoporous alumina	7.5–1500	5	5	121	47	18
$Al(OH)CO_3$	1–500	0.5	7	45	7	51
Flower-like MgO	1–400	0.3	7	343.64	252.34	22
Fe_3O_4 nanoparticles	0.025–25	0.5	8	180	160	32
γ-Fe_2O_3@ carbon	0.2–30	1	7	29.4	17.9	52
Zr–Mn binary oxide	5–40	0.2	5	80	104	53

Fig. S7 (ESI†) illustrates the adsorption isotherms of As(v) on the crystalline samples calcined at 900 °C. Table S4 (ESI†) shows the adsorption isotherm parameters. The adsorption capacities of the crystalline composite samples are substantially lower than those of the amorphous counterparts because of a reduction in surface areas and hence quantity of functional groups after high temperature calcination. For instance, the As(v) adsorption capacity of mesoporous alumina decreases by 74%. Therefore, the following adsorption studies focus on the composite samples calcined at 400 °C.

The adsorption capacities of the mesoporous aluminium magnesium oxide adsorbents for As(iii) were also studied. Fig. 4d displays the adsorption isotherms of As(iii) over the composite samples at an initial pH of 7. The adsorption isotherm parameters are given in Table S5, ESI.† The As(iii) adsorption data fit the Langmuir model better for meso-Al-400 and meso-Mg-400. The adsorption capacities of As(iii) on all the amorphous mesoporous composites are lower than those of As(v), suggesting that arsenite is more difficult to adsorb than arsenate. The highest As(iii) adsorption capacity of pure meso-Al-400 is 114.8 mg g^{-1} at the initial arsenic concentration of 820 mg L^{-1}. The incorporation of Mg enhances the As(iii) adsorption. The observed trend of the As(iii) adsorption capacities is quite similar to that of the As(v) adsorption. The highest As(iii) adsorption capacity of the composites is 390.6 mg g^{-1}, achieved by the meso-80Al20-400 sample. More importantly, meso-Mg-400 shows a remarkable As(iii) adsorption capacity of 848 mg g^{-1}, indicating that the mesoporous magnesium oxide is an extraordinary adsorbent for removing both inorganic As(v) and As(iii) species. This is the highest As(iii) adsorption capacity compared with reported adsorbents under neutral pH environment (Table 2). The composite adsorbents appear to adsorb the arsenite directly and show excellent arsenite uptake without oxidation pre-treatment. These results for the adsorption of As(v) and As(iii) demonstrate that the as-synthesized mesoporous aluminium magnesium oxide composites are highly efficient adsorbents for the removal of toxic arsenic from water.

The pH value of the water bodies can significantly influence the arsenic adsorption performance of adsorbents, because the arsenic species distribution and their interaction with adsorbents are pH-dependent. The effect of the initial pH of the arsenic solution on the uptake capacities was investigated. The experiment was carried out with meso-Al-400, meso-80Al20Mg-400 and meso-Mg-400 by varying the initial pH from 2 to 12 with an initial concentration of As(v) or As(iii) of 400 mg L^{-1}. For all three samples, the As(v) adsorption capacity significantly increases when the initial pH rises from 2 to 3, and then gradually decreases when increasing the pH to 12 (Fig. 5a–c). The highest As(v) adsorption capacities at pH 3 were 214 mg g^{-1} for meso-Al-400, 331 mg g^{-1} for meso-80Al20Mg-400, and 733 mg g^{-1} for meso-Mg-400. For As(iii), the trend is slightly different. The As(iii) adsorption capacities remain constant at *ca.* 150 mg g^{-1} for meso-Al-400 in the pH range of 5–10, at *ca.* 250 mg g^{-1} for meso-80Al20Mg-400 in the pH range of 4.0–9.4, and at *ca.* 610 mg g^{-1} for meso-Mg-400 in the pH range of 3.0–10.4. The As(iii) adsorption capacities decrease beyond these pH ranges.

This pH-dependent behavior is related to the surface charge of the adsorbents, variation in the arsenic speciation

Published on 21 October 2015. Downloaded on 18/03/2016 08:24:55.

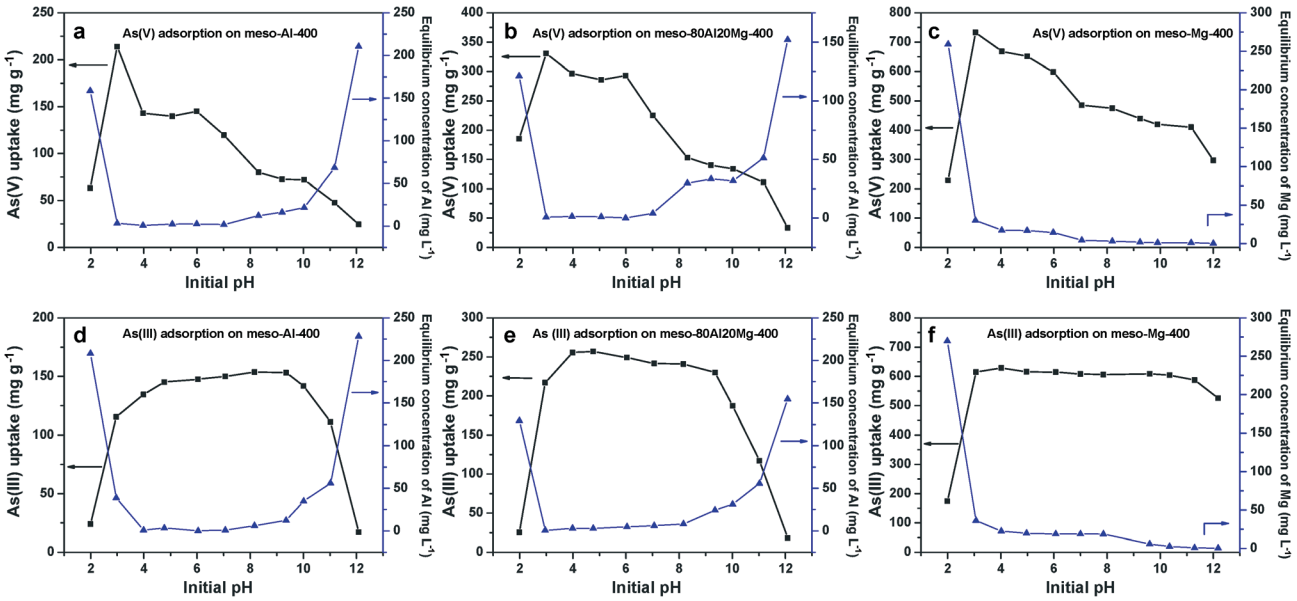

Fig. 5 Effect of the initial pH on the As(v) adsorption capacities of (a) meso-Al-400, (b) meso-80Al20Mg-400 and (c) meso-Mg-400; effect of the initial pH on the As(III) adsorption capacities of (d) meso-Al-400, (e) meso-80Al20Mg-400 and (f) meso-Mg-400. Also graphed is the Al or Mg equilibrium concentration of the solution, an indicator of the dissolution of the adsorbent. Experimental conditions: dose = 0.5 g L^{-1}, initial concentration of either As(v) or As(III) = 400 mg L^{-1}.

at different pH values, and possible partial dissolution of the adsorbents. On one hand, the arsenic solution pH affects the surface charge of the solid adsorbents. The pH_{zpc} is an intrinsic property of a solid–liquid interface, which reflects the charge of the surface. It is mainly determined by surface chemistry and the crystallinity of the solid.[18] Table 1 summarizes the pH_{zpc} values of the composite adsorbents calcined at 400 °C. The pH_{zpc} increases from 8.3 to higher than 13 with increasing Mg content. The pH_{zpc} for alumina and MgO have been reported in the range of 8–10 and 12.4, respectively.[8,22] When the solution pH is lower than the pH_{zpc}, the surface of the oxide adsorbents is positively charged due to the presence of abundant protonated hydroxyl groups, which is favorable for the adsorption of anions *via* electrostatic interaction.[37] On the other hand, the solution pH influences the As(v)/As(III) speciation, as presented in Fig. S8, ESI.†[54–56] The predominant As(v) species are negatively charged, $H_2AsO_4^-$, $HAsO_4^{2-}$ and AsO_4^{3-}, in the pH range of 2–6, 6–11 and 11–14, respectively.[54] With increasing pH from 3 to the corresponding pH_{zpc} of the adsorbent, the electrostatic attraction between positively charged adsorbents and negatively charged As(v) species decreases, resulting in the gradual decline in the adsorption capacities for As(v) on meso-Al-400, meso-80Al20Mg-400 and meso-Mg-400. When the solution pH is higher than the pH_{zpc}, the adsorbent surface will be negatively charged and electrostatic repulsion occurs between the adsorbent surface and the negatively charged As(v) species ($HAsO_4^{2-}$ and AsO_4^{3-} above pH 8.0), leading to decreasing As(v) adsorption capacities. The pH_{zpc} moves to higher pH values with increasing Mg content in the mesoporous composites and thus facilitates the electrostatic attraction to arsenic species, improving the adsorption performance. For As(III), neutral H_3AsO_3 dominates for pH < 9.2. The electrostatic interaction between positively charged adsorbents and negatively charged As(v) species is stronger than that of neutral H_3AsO_3, giving rise to higher adsorption capacities for As(v) especially in the pH range of 2–6. That is why As(III) is more difficult to adsorb.[20,54,56] In contrast, when the pH is higher than 9, the predominant As(III) species are negatively charged: $H_2AsO_3^-$, $HAsO_3^{2-}$ and AsO_3^{3-}. Thus electrostatic repulsion causes the decline in As(III) adsorption capacities on the mesoporous aluminium magnesium oxide adsorbents.

In strongly acidic (pH < 2) or alkaline (pH > 8) solutions, alumina is partially dissolved, degrading the adsorbent and releasing Al ions into the solution and hence decreasing arsenic uptake capacities (Fig. 5a, b, d and e). The meso-Mg-400 sample is slightly dissolved (<12%) in the pH range of 3–12. In this case, the electrostatic interactions play a more significant role in the arsenic adsorption as discussed above. However, the meso-Mg-400 sample is substantially dissolved (>85%) at an initial pH of 2, resulting in a dramatic decline in the As(v) and As(III) adsorption capacities. The initial pH of the arsenic solution greatly influences the surface charge of the adsorbents, the arsenic speciation and dissolution of the adsorbents. Consequently, the arsenic adsorption performance of the adsorbents greatly depends on the pH of the water bodies. Thus the pH adjustment process is usually required to achieve effective removal of arsenic in practical water treatment.

The above results demonstrate that the as-prepared mesoporous aluminium magnesium oxide composites are highly efficient adsorbents for the removal of arsenic with excellent results obtained over a wide pH range. Meso-Mg-400 has high

 This journal is © The Royal Society of Chemistry 2016

Published on 21 October 2015. Downloaded on 18/03/2016 08:24:55.

adsorption capacities for As(v) (485 mg g^{-1}) and As(iii) (608 mg g^{-1}) at pH 7.0 in 400 mg L^{-1} arsenic. Adjustment of the pH and pre-oxidation processes are not required for arsenic adsorption on these composite adsorbents.

Natural underground water and wastewater contain many other anions, such as nitrate, sulphate and phosphate, which may compete with arsenic for the active adsorption sites.[57] Thus the effect of coexisting anions on the As(v) adsorption capacities of four samples (meso-Al-400, meso-80Al20Mg-400, meso-70Al30Mg-400 and meso-Mg-400) was investigated at an initial pH of 6.0 and an initial concentration of 50 mg L^{-1} of As(v). There is no substantial impact on the As(v) adsorption capacities over these four adsorbents in the presence of NO_3^-, Cl^-, SO_4^{2-} and CO_3^{2-} (Fig. S9, ESI†) with the As(v) removal remaining over 97%. The silicate and phosphate anions had a slight negative effect on the arsenic uptake capacities of meso-Al-400, meso-80Al20Mg-400 and meso-70Al30Mg-400, because they have high negative charge and affinity to aluminium-based adsorbents.[4,5] For instance, the arsenic uptake capacities of meso-70Al30Mg-400 decreases by 7% and 18% in the presence of 50 mg L^{-1} of SiO_3^{2-} and PO_4^{3-}, respectively. However, SiO_3^{2-} and PO_4^{3-} do not affect the adsorption capacities of meso-Mg-400 for As(v), with 99% arsenic removal. The excellent selectivity for As(v) indicates that the electrostatic interaction is not the sole adsorption mechanism, as other competing anions would also electrostatically bond. The chemisorption binding affinity to the arsenate is likely to dominate when an initial pH of 6.0 was used and in the presence of interfering anions, which will be discussed later. The aluminium magnesium oxide composites have demonstrated high selectivity for arsenic, showing potential for purification of complex water bodies.

The adsorption capacities of meso-Al-400, meso-80Al20Mg-400 and meso-Mg-400 for both As(v) and As(iii) are compared with those of other adsorbents reported in the literature (Table 2). The mesoporous samples, especially meso-Mg-400, exhibit significantly higher adsorption capacities for As(v) and As(iii). For example, the adsorption capacities of meso-Mg-400 for As(v) and As(iii) are 74 times and 233 times higher, respectively, than those of commercial activated alumina adsorbents under similar pH conditions.[43] In addition, few studies tested the arsenic adsorption performance over a wide pH range or in the presence of co-existing ions. However, the mesoporous aluminium magnesium oxide composites demonstrate unprecedentedly high adsorption capacities for As(v) and As(iii) over a wide pH range.

Arsenic adsorption mechanism

In order to determine the adsorption mechanism of arsenic onto the composite adsorbents, meso-Al-400, meso-80Al20Mg-400 and meso-Mg-400 were characterized by TEM, XRD, XPS and Fourier-transform infrared spectroscopy (FTIR) after arsenic adsorption. The TEM images (Fig. S10a and b, ESI†) show that both meso-Al-400 and meso-80Al20Mg-400 still retained the hexagonally ordered mesoporous frameworks after adsorption of As(v), indicating the structure is robust. Nevertheless, the meso-Mg-400 became nanosheet agglomerate and the original wormhole-like mesopores composed of primary nanoparticles disappeared after As(v) adsorption (Fig. S10 c–d, ESI†).

The XRD patterns (Fig. S11, ESI†) demonstrate that meso-Al-400 and meso-80Al20Mg-400 were still amorphous after adsorption of either As(v) or As(iii), while meso-Mg-400 was converted to $Mg(OH)_2$ as well as some unindexed phase that is perhaps a magnesium–arsenic hydroxide compound. MgO could react with water to form $Mg(OH)_2$ with more hydroxyl groups, as previously reported in the literature.[22,44,48,58] Then the resulting $Mg(OH)_2$ may interact with arsenate or arsenite to form compounds. Due to the broadened diffraction peaks and poor crystallinity of the resulting compounds, these peaks cannot be clearly indexed to any JCPDS cards. Similar compounds were also observed in previous literature reports, where it was assumed that the as-formed compounds were magnesium arsenate/arsenite.[44,58]

XPS spectra (Fig. S12 and S13, ESI†) of meso-Al-400, meso-80Al20Mg-400 and meso-Mg-400 were obtained after adsorption of 400 mg L^{-1} of As(v) or As(iii). The XPS spectra (Fig. S12, ESI†) confirm the presence of As adsorbed on the surface. For meso-Al-400 and meso-80Al20Mg-400, the Al 2p peaks (Fig. S13a and d, ESI†) are located at 74.75 eV and 74.65 eV, respectively, which is similar to activated alumina.[8] After As(v) adsorption, the Al 2p peaks shift towards lower binding energy. In contrast, the Al 2p peaks move slightly towards higher binding energy after As(iii) adsorption. This indicates interaction between As species and Al.[59,60] The divergence of the Al 2p peak after adsorption of As(v) or As(iii) over meso-Al-400 and meso-80Al20Mg-400 is likely due to the different initial pH for adsorption of arsenate ($H_2AsO_4^-$ at pH 3.0) and arsenite ($H_3AsO_3^0$ at pH 7.0). This will affect the dominant arsenic speciation and surface complexes (inner-sphere or outer-sphere complexes) formed between aluminium and arsenic, possibly resulting in the divergent shift (see details in ESI†).[61–63] After adsorption of As(v), the Mg 2p peak (Fig. S13g, ESI†) of meso-Mg-400 at 50.6 eV is attributed to Mg species in the form of Mg–O–As.[22] Whereas, after As(iii) adsorption, the Mg 2p peak (Fig. S13h, ESI†) shifts to 49.6 eV and can be convoluted into two peaks; 49.4 eV (Mg–O–H) and 50.3 eV (Mg–O–As).[64] This suggests the formation of $Mg(OH)_2$ from the reaction between MgO and water in good agreement with the XRD results.[22,44] As a peak associated with Mg–O–H was not observed in the presence of As(v) species, the As(v) adsorption can be assumed to have replaced the surface hydroxyl groups, forming Mg–O–As, while As(iii) species only bond with some of the hydroxyl groups to form Mg–O–As, leaving residual Mg–O–H owing to their weak affinity to hydroxyl group.[22] For meso-80Al20Mg-400, the Mg 2p peaks (Fig. S13e and f, ESI†) after adsorption of As(v) and As(iii) are located at 50.4 eV and 50.8 eV, respectively, which can be assigned to Mg–O–As without residual Mg–O–H. Strong As 3d peaks (Fig. S13 b–h, ESI†) in meso-Al-400, meso-80Al20Mg-400 and meso-Mg-400 are observed, indicating high As

Published on 21 October 2015. Downloaded on 18/03/2016 08:24:55.

loading. After adsorption of As(III), the As 3d peaks of meso-Al-400 and meso-80Al20Mg-400 can be convoluted into two peaks located at ~44.8 eV and ~45.9 eV, which can be attributed to As(III)–O and As(V)–O, respectively.[65] This indicates that some of As(III) is oxidized to As(V) during the adsorption process. For meso-Mg-400, the As 3d peak is located at 44.5 eV and no oxidation of As(III) is observed.[48] After adsorption of As(V), only one As 3d peak is observed at *ca.* 45.9 eV which belongs to As(V)–O.[22]

The surface metal compositions of meso-Al-400, meso-80Al20Mg-400 and meso-Mg-400 before and after As(V) or As(III) adsorption were determined by XPS, as shown in Table S6, ESI.† For the meso-80Al20Mg-400, the atomic ratio of Al/Mg is 4.5, which is close to the bulk Al/Mg atomic ratio obtained by ICP-OES and the expected theoretical Al/Mg ratio from the feeding ratio. This indicates that there is no substantial Al-rich or Mg-rich phase on the surface, and that the Al and Mg are uniformly mixed in the composite. However, after adsorption of As(V) at pH 3 or adsorption of As(III) at pH 7, the Al/Mg ratio in the meso-80Al20Mg-400 was changed to 9.3 and 9.9 respectively, indicating the leaching of Mg from the surface (some *in situ* formed $Mg(OH)_2$ dissolved) during the adsorption process, similar to the observation in the reported MgAl layered double hydroxides.[66]

Two research groups revealed the interaction of arsenate/arsenite with commercial bulky $Al(OH)_3$ and MgO, respectively, by using extended X-ray adsorption fine structure (EXAFS) and X-ray absorption near edge structure (XANES) techniques.[48,60] As(V) was bound to $Al(OH)_3$ by bidentate binucleate As–O–Al bonding. As(III) formed layers and/or chains of AsO_3 pyramids that were weakly adsorbed onto $Mg(OH)_2$ surface, while As(V) was strongly bound to $Mg(OH)_2$ by mondentate As–O–Mg bonding. This can explain our observations about the adsorption performance differences and XPS results. Based on the current results, it is proposed that the arsenic adsorption mechanism includes a combination of inner-sphere surface complexes (chemical bonding) and outer-sphere complexes (electrostatic interaction) under the present experimental conditions, consistent with previous publications.[61–63,67] Future work will focus on the underlying adsorption mechanism (specific surface complexation configurations) of our adsorbents with extremely high adsorption capacities for arsenic by EXAFS and XANES.

The FTIR spectra (Fig. S14, ESI†) of the dry composite adsorbents give further information about the adsorption mechanism. For pristine meso-Al-400 and meso-80Al20Mg-400, the characteristic broad peak of hydroxyl groups in alumina centered at around 3500 cm^{-1} is observed. After adsorption of As(III) or As(V), the intensity of this broad peak decreases, indicating the participation of hydroxyl groups in the adsorption of arsenic. Particularly the intensity declines significantly after adsorption of As(V), suggesting that hydroxyl groups are replaced to bond As(V), resulting in higher adsorption capacities for As(V). The intensity slightly decreases after adsorption of As(III), because the affinity of As(III) with hydroxyl groups is weaker. It is difficult to distinguish the As–O bond peak due to overlap with the Al–O peak.[68] For meso-Mg-400, besides the broad hydroxyl peak, one sharp and strong peak at 3700 cm^{-1} can be observed after adsorption of As(III), which is attributed to hydroxyl stretching vibration in the as-formed $Mg(OH)_2$.[22] The peak at 3700 cm^{-1} is hardly observed after adsorption of As(V). This demonstrates that As(V) is prone to form Mg–O–As by replacing most surface hydroxyl groups. By contrast, residual –OH remains (peak at 3700 cm^{-1}) in the case of As(III) adsorption, because of the weak affinity of As(III) to hydroxyl groups. Furthermore, a new peak appears at 841 cm^{-1} and 819 cm^{-1} after adsorption of As(V) and As(III), respectively. These peaks can be assigned to the vibration of As–O.[69]

Based on the above results, it is proposed that the hydroxyl groups on the adsorbents play a critical role in the As(V)/As(III) adsorption efficiency and capacity. For meso-Al-400, the abundant, accessible hydroxyl groups give rise to high adsorption for As with good retention of ordered mesoporous framework. The meso-Mg-400 is endowed with more hydroxyl groups after it reacts with water, which results in structure conversion from MgO nanoparticles to $Mg(OH)_2$ nanosheet agglomerate. The whole arsenic removal process involves reaction of MgO with water, adsorption of As(V)/As(III) onto $Mg(OH)_2$ and reaction between $Mg(OH)_2$ and arsenate/arsenite, which contributes to extremely high adsorption capacities for both As(V) and As(III). It should be noted that the electrostatic attraction between positively charged adsorbents and negatively charged As species also facilitates the adsorption of As onto the adsorbents as mentioned before.

In terms of recyclability and reuse, the desorption of arsenic from the used composite adsorbent was not satisfactory, due to the strong affinity of arsenic onto the adsorbents as mentioned above. However, Tresintsi *et al.* reported that some of these composite adsorbents once used, such as arsenic-saturated MgO/$Mg(OH)_2$, can be utilized as environmentally benign additives in cement building, which offers alternative application of the used adsorbents.[48]

Conclusions

In summary, mesoporous aluminium oxide, magnesium oxide and their composites have been synthesized by a facile, low-cost and scalable sol–gel method. The Mg/Al molar ratio of the composites were varied and high surface area materials (118–425 $m^2\ g^{-1}$) were obtained. The mesopores of the composites evolve from a hexagonally ordered structure to a wormhole-like structure with increasing Mg/Al ratio. The correlation of the composite properties including the composition, pH_{zpc}, crystallinity and mesostructure with the arsenic adsorption performance was systematically studied. Due to the high surface areas, large pore volumes, high pH_{zpc} and high quantities of accessible hydroxyl groups with strong chemisorption binding affinity to arsenic, the mesoporous aluminium magnesium oxide composites show extremely high adsorption capacities for As(V) and As(III) over a wide pH range and excellent selectivity in the presence of co-existing

 This journal is © The Royal Society of Chemistry 2016

Published on 21 October 2015. Downloaded on 18/03/2016 08:24:55.

anions. The maximum adsorption capacities of mesoporous magnesia are 912 mg g^{-1} for As(v) at pH 3 and 813 mg g^{-1} for As(III) at pH 7, which are the highest reported adsorption capacities for As so far. The zeta potential, TEM, XRD, XPS and FTIR results gave an insight into the arsenic adsorption mechanism that involves formation of hydroxide (for magnesia), electrostatic attraction and adsorption through the hydroxyl group under the current experimental conditions. This study introduces a feasible approach towards the rational design and fabrication of cost-effective yet highly efficient adsorbents. The unprecedentedly high adsorption capacities and superior selectivity make the mesoporous aluminium magnesium oxide composites promising candidates for practical water treatment.

Acknowledgements

This project received financial support from Joint Research Project funding (GJHZ1224) from Chinese Academy of Sciences (CAS) and the Commonwealth Scientific and Industrial Research Organisation (CSIRO). We acknowledge the Australian Synchrotron for access to the SAXS beamline through the Science and Industry Endowment Fund Special Research Program – Synchrotron Science. Winston Liew, Mark Hickey and Yesim Gozukara (CSIRO) are thanked for the ICP-OES measurements. The CSIRO Office of the Chief Executive (OCE) Postdoctoral and Science Leader Schemes are acknowledged for supporting this work. R. A. C. acknowledges the Australian Research Council for a Future Fellowship (FT0990583).

Notes and references

1 EPA, *EPA's Terms of Environment: Glossary, Abbreviations, and Acronyms*, USA Environmental Protection Agency, 2009.
2 J. Li, *Nature*, 2013, **499**, 14–15.
3 J. O. Nriagu, *Science*, 1996, **272**, 223.
4 S. Babel and T. Kurniawan, *J. Hazard. Mater.*, 2003, **97**, 219–243.
5 I. Ali, *Chem. Rev.*, 2012, **112**, 5073–5091.
6 X. Gao, L.-P. Xu, Z. Xue, L. Feng, J. Peng, Y. Wen, S. Wang and X. Zhang, *Adv. Mater.*, 2014, **26**, 1771–1775.
7 W. Li, F. Xia, J. Qu, P. Li, D. Chen, Z. Chen, Y. Yu, Y. Lu, R. Caruso and W. Song, *Nano Res.*, 2014, **7**, 903–916.
8 W. Li, C.-Y. Cao, L.-Y. Wu, M.-F. Ge and W.-G. Song, *J. Hazard. Mater.*, 2011, **198**, 143–150.
9 WHO, *Guidelines for drinking-water quality*, 2011.
10 S. Fendorf, H. A. Michael and A. Geen, *Science*, 2010, **328**, 1123–1127.
11 L. Rodríguez-Lado, G. Sun, M. Berg, Q. Zhang, H. Xue, Q. Zheng and C. A. Johnson, *Science*, 2013, **341**, 866–868.
12 M. Amini, K. C. Abbaspour, M. Berg, L. Winkel, S. J. Hug, E. Hoehn, H. Yang and C. A. Johnson, *Environ. Sci. Technol.*, 2008, **42**, 3669–3675.
13 H. A. Michael, *Science*, 2013, **341**, 852–853.
14 G. Sun, Y. Xu, Q. Zheng and S. Xi, *Kaohsiung J. Med. Sci.*, 2011, **27**, 377–381.
15 G. Sun, *Toxicol. Appl. Pharmacol.*, 2004, **198**, 268–271.
16 P. Ravenscroft, H. Brammer and K. Richards, *Arsenic Pollution: A Global Synthesis*, Wiley-Blackwell, USA, 2009, pp. 157–212.
17 W. R. Cullen and K. J. Reimer, *Chem. Rev.*, 1989, **89**, 713–764.
18 Y. Kim, C. Kim, I. Choi, S. Rengaraj and J. Yi, *Environ. Sci. Technol.*, 2004, **38**, 924–931.
19 P. L. Smedley and D. G. Kinniburgh, *Appl. Geochem.*, 2002, **17**, 517–568.
20 J. Yang, H. Zhang, M. Yu, I. Emmanuelawati, J. Zou, Z. Yuan and C. Yu, *Adv. Funct. Mater.*, 2013, **24**, 1354–1363.
21 B. A. Manning and S. Goldberg, *Environ. Sci. Technol.*, 1997, **31**, 2005–2011.
22 X.-Y. Yu, T. Luo, Y. Jia, Y.-X. Zhang, J.-H. Liu and X.-J. Huang, *J. Phys. Chem. C*, 2011, **115**, 22242–22250.
23 M. M. Pendergast and E. M. V. Hoek, *Energy Environ. Sci.*, 2011, **4**, 1946–1971.
24 V. K. Gupta, I. Ali, T. A. Saleh, A. Nayak and S. Agarwal, *RSC Adv.*, 2012, **2**, 6380–6388.
25 J. C. Crittenden, R. R. Trussell, D. W. Hand, K. J. Howe and G. Tchobanoglous, *MWH's Water Treatment: Principles and Design*, John Wiley & Sons, USA, 2012.
26 M. Li, C. Wang, M. J. O'Connell and C. K. Chan, *Environ. Sci.: Nano*, 2015, **2**, 245–250.
27 L. S. Zhong, J. S. Hu, H. P. Liang, A. M. Cao, W. G. Song and L. J. Wan, *Adv. Mater.*, 2006, **18**, 2426–2431.
28 B. Wang, H. Wu, L. Yu, R. Xu, T.-T. Lim and X. W. Lou, *Adv. Mater.*, 2012, **24**, 1111–1116.
29 H. Li, W. Li, Y. Zhang, T. Wang, B. Wang, W. Xu, L. Jiang, W. Song, C. Shu and C. Wang, *J. Mater. Chem.*, 2011, **21**, 7878–7881.
30 L.-S. Zhong, J.-S. Hu, L.-J. Wan and W.-G. Song, *Chem. Commun.*, 2008, 1184–1186.
31 B. Paul, V. Parashar and A. Mishra, *Environ. Sci.: Water Res. Technol.*, 2015, **1**, 77–83.
32 C. T. Yavuz, J. T. Mayo, W. W. Yu, A. Prakash, J. C. Falkner, S. Yean, L. Cong, H. J. Shipley, A. Kan, M. Tomson, D. Natelson and V. L. Colvin, *Science*, 2006, **314**, 964–967.
33 C.-Y. Cao, Z.-M. Cui, C.-Q. Chen, W.-G. Song and W. Cai, *J. Phys. Chem. C*, 2010, **114**, 9865–9870.
34 X.-Y. Yu, R.-X. Xu, C. Gao, T. Luo, Y. Jia, J.-H. Liu and X.-J. Huang, *ACS Appl. Mater. Interfaces*, 2012, **4**, 1954–1962.
35 V. Chandra, J. Park, Y. Chun, J. W. Lee, I.-C. Hwang and K. S. Kim, *ACS Nano*, 2010, **4**, 3979–3986.
36 J. Zhu, S. A. Baig, T. Sheng, Z. Lou, Z. Wang and X. Xu, *J. Hazard. Mater.*, 2015, **286**, 220–228.
37 S. A. Ntim and S. Mitra, *J. Colloid Interface Sci.*, 2012, **375**, 154–159.
38 C. Jing, J. Cui, Y. Huang and A. Li, *ACS Appl. Mater. Interfaces*, 2012, **4**, 714–720.
39 X. Yang, X. Wang, Y. Feng, G. Zhang, T. Wang, W. Song, C. Shu, L. Jiang and C. Wang, *J. Mater. Chem. A*, 2013, **1**, 473–477.
40 Y.-X. Zhang, X.-Y. Yu, Z. Jin, Y. Jia, W.-H. Xu, T. Luo, B.-J. Zhu, J.-H. Liu and X.-J. Huang, *J. Mater. Chem.*, 2011, **21**, 16550–16557.

Published on 21 October 2015. Downloaded on 18/03/2016 08:24:55.

41 Q. Yuan, A.-X. Yin, C. Luo, L.-D. Sun, Y.-W. Zhang, W.-T. Duan, H.-C. Liu and C.-H. Yan, *J. Am. Chem. Soc.*, 2008, **130**, 3465–3472.
42 S. M. Morris, P. F. Fulvio and M. Jaroniec, *J. Am. Chem. Soc.*, 2008, **130**, 15210–15216.
43 T.-F. Lin and J.-K. Wu, *Water Res.*, 2001, **35**, 2049–2057.
44 Y. Liu, Q. Li, S. Gao and J. K. Shang, *J. Am. Ceram. Soc.*, 2011, **94**, 217–223.
45 C.-Y. Cao, J. Qu, F. Wei, H. Liu and W.-G. Song, *ACS Appl. Mater. Interfaces*, 2012, **4**, 4283–4287.
46 J. Hu, Z. Song, L. Chen, H. Yang, J. Li and R. Richards, *J. Chem. Eng. Data*, 2010, **55**, 3742–3748.
47 S.-W. Bian, J. Baltrusaitis, P. Galhotra and V. H. Grassian, *J. Mater. Chem.*, 2010, **20**, 8705–8710.
48 S. Tresintsi, K. Simeonidis, M. Katsikini, E. C. Paloura, G. Bantsis and M. Mitrakas, *J. Hazard. Mater.*, 2014, **265**, 217–225.
49 I. Langmuir, *J. Am. Chem. Soc.*, 1916, **38**, 2221–2295.
50 H. Freundlich, *Z. Phys. Chem.*, 1906, **57**, 385–470.
51 C.-Y. Cao, P. Li, J. Qu, Z.-F. Dou, W.-S. Yan, J.-F. Zhu, Z.-Y. Wu and W.-G. Song, *J. Mater. Chem.*, 2012, **22**, 19898–19903.
52 Z. Wu, W. Li, P. A. Webley and D. Zhao, *Adv. Mater.*, 2012, **24**, 485–491.
53 G. Zhang, A. Khorshed and J. Paul Chen, *J. Colloid Interface Sci.*, 2013, **397**, 137–143.
54 P. Ravenscroft, H. Brammer and K. Richards, *Arsenic Pollution: A Global Synthesis*, Wiley-Blackwell, USA, 2009, pp. 25–72.
55 X. Meng, S. Bang and G. P. Korfiatis, *Water Res.*, 2000, **34**, 1255–1261.
56 K. R. Henke and A. Hutchison, *Arsenic: Environmental Chemistry, Health Threats and Waste Treatment*, John Wiley & Sons, USA, 2009, pp. 9–68.
57 Y. Jia, X.-Y. Yu, T. Luo, Z. Jin, B. Sun, J.-H. Liu and X.-J. Huang, *Dalton Trans.*, 2014, **43**, 2348–2351.
58 Y. Jia, T. Luo, X.-Y. Yu, B. Sun, J.-H. Liu and X.-J. Huang, *RSC Adv.*, 2013, **3**, 5430–5437.
59 K.-H. Goh, T.-T. Lim and Z. Dong, *Environ. Sci. Technol.*, 2009, **43**, 2537–2543.
60 P. Kappen and J. Webb, *Appl. Geochem.*, 2013, **31**, 79–83.
61 C. Hu, Q. Chen, H. Liu and J. Qu, *J. Hazard. Mater.*, 2015, **293**, 97–104.
62 G. Durate, V. S. T. Ciminelli, M. S. S. Dantas, H. A. Durate, I. F. Vasconcelos, A. F. Oliveira and K. Osseo-Asare, *Geochim. Cosmochim. Acta*, 2012, **83**, 205–216.
63 A. C. Q. Ladeira, V. S. T. Ciminelli, H. A. Durate, M. C. M. Alves and A. Y. Ramos, *Geochim. Cosmochim. Acta*, 2001, **65**, 1211–1217.
64 S. Ardizzone, C. L. Bianchi, M. Fadoni and B. Vercelli, *Appl. Surf. Sci.*, 1997, **119**, 253–259.
65 S. Zhang, H. Niu, Y. Cai, X. Zhao and Y. Shi, *Chem. Eng. J.*, 2010, **158**, 599–607.
66 X. Wu, X. Tan, S. Yang, T. Wen, H. Guo, X. Wang and A. Xu, *Water Res.*, 2013, **47**, 4159.
67 J. G. Catalano, C. Park, P. Fenter and Z. Zhang, *Geochim. Cosmochim. Acta*, 2008, **72**, 1986–2004.
68 H. Li, L. Zhang, H. Dai and H. He, *Inorg. Chem.*, 2009, **48**, 4421–4434.
69 M. Pena, X. Meng, G. P. Korfiatis and C. Jing, *Environ. Sci. Technol.*, 2006, **40**, 1257–1262.

 This journal is © The Royal Society of Chemistry 2016